

# Ultrathin $\text{Hf}_{0.5}\text{Zr}_{0.5}\text{O}_2$ Ferroelectric Films on Si

Anna Chernikova,<sup>†</sup> Maksim Kozodaev,<sup>†</sup> Andrei Markeev,<sup>†</sup> Dmitrii Negrov,<sup>†</sup> Maksim Spiridonov,<sup>†</sup> Sergei Zarubin,<sup>†</sup> Ohheum Bak,<sup>‡</sup> Pratyush Buragohain,<sup>‡</sup> Haidong Lu,<sup>‡</sup> Elena Suvorova,<sup>‡</sup> Alexei Gruverman,<sup>\*,‡</sup> and Andrei Zenkevich<sup>\*,†,‡</sup>

<sup>†</sup>Moscow Institute of Physics and Technology, Dolgoprudny, Moscow Region 141700, Russia

<sup>‡</sup>Department of Physics and Astronomy, University of Nebraska, Lincoln, Nebraska 68588-0299, United States

<sup>\*</sup>École Polytechnique Fédérale de Lausanne, Lausanne, CH-1015, Switzerland

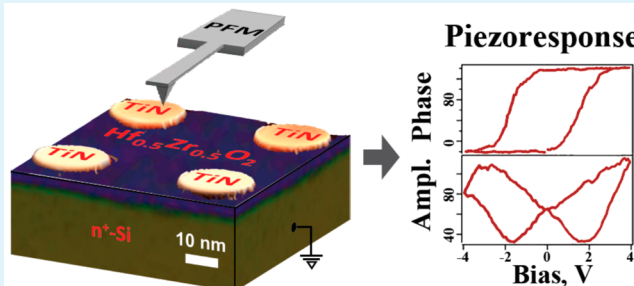
<sup>||</sup>A.V. Shubnikov Institute of Crystallography, Leninsky pr. 59, Moscow 119333, Russia

<sup>\*</sup>NRNU “Moscow Engineering Physics Institute”, Moscow 115409, Russia

## S Supporting Information

**ABSTRACT:** Because of their immense scalability and manufacturability potential, the  $\text{HfO}_2$ -based ferroelectric films attract significant attention as strong candidates for application in ferroelectric memories and related electronic devices. Here, we report the ferroelectric behavior of ultrathin  $\text{Hf}_{0.5}\text{Zr}_{0.5}\text{O}_2$  films, with the thickness of just 2.5 nm, which makes them suitable for use in ferroelectric tunnel junctions, thereby further expanding the area of their practical application. Transmission electron microscopy and electron diffraction analysis of the films grown on highly doped Si substrates confirms formation of the fully crystalline non-centrosymmetric orthorhombic phase responsible for ferroelectricity in  $\text{Hf}_{0.5}\text{Zr}_{0.5}\text{O}_2$ . Piezoresponse force microscopy and pulsed switching testing performed on the deposited top TiN electrodes provide further evidence of the ferroelectric behavior of the  $\text{Hf}_{0.5}\text{Zr}_{0.5}\text{O}_2$  films. The electronic band lineup at the top  $\text{TiN}/\text{Hf}_{0.5}\text{Zr}_{0.5}\text{O}_2$  interface and band bending at the adjacent  $n^+$ -Si bottom layer attributed to the polarization charges in  $\text{Hf}_{0.5}\text{Zr}_{0.5}\text{O}_2$  have been determined using in situ X-ray photoelectron spectroscopy analysis. The obtained results represent a significant step toward the experimental implementation of Si-based ferroelectric tunnel junctions.

**KEYWORDS:** hafnium oxides, ultrathin films, ferroelectric switching, CMOS integration, ferroelectric tunnel junctions



## INTRODUCTION

Ferroelectric (FE) thin films have enormous potential for technological applications, particularly in data storage and memory devices, because of the electrically switchable spontaneous polarization. Recent experimental and theoretical investigations show that under appropriate mechanical and electric boundary conditions ferroelectricity may persist for the film thickness down to just several unit cells.<sup>1–5</sup> Besides the academic interest, these experimental and theoretical findings opened a possibility of an alternative nonvolatile memory concept based on polarization-controlled electroresistance effect in the devices termed ferroelectric tunnel junctions (FTJs).<sup>6,7</sup> FTJs incorporate a FE barrier, which is thin enough to allow direct electron tunneling between two electrodes with different work functions. Polarization reversal in the FE barrier alters the tunneling resistance due to changes in the asymmetric potential profile or/and in the density of states at the barrier/electrode interfaces.<sup>6,7</sup> The experimental realization of FTJs has been demonstrated mostly by employing heteroepitaxial ferroelectric perovskite films as a tunnelling barrier sandwiched

between metallic, conductive oxide, or semiconducting electrodes.<sup>4,8–12</sup>

Recently, the FE properties have been discovered in the polycrystalline  $\text{HfO}_2$  thin films doped with different elements.<sup>13–15</sup> Although the origin of ferroelectricity is still debated, most of the theoretical<sup>16</sup> and experimental<sup>17,18</sup> studies assign their ferroelectric behavior to the non-centrosymmetric orthorhombic  $\text{HfO}_2$  phase ( $Pbc_2$  symmetry), which crystallizes during high-temperature annealing and is metastable at room temperature. The stabilization of the FE phase in polycrystalline  $\text{HfO}_2$  films was shown to depend on various parameters, such as dopant species and their concentration, film thickness, and conditions of thermal treatment. In particular, it was found that a relatively high thermal budget in the temperature range between 650 and 1000 °C is required.<sup>13</sup> Alternatively, the FE properties have been observed in the alloyed  $\text{Hf}_x\text{Zr}_{1-x}\text{O}_y$  thin films, with the most robust effect reported for the  $\text{Hf}_{0.5}\text{Zr}_{0.5}\text{O}_2$

Received: December 25, 2015

Accepted: March 2, 2016

Published: March 2, 2016



composition.<sup>19</sup> The temperature required to crystallize  $\text{Hf}_{0.5}\text{Zr}_{0.5}\text{O}_2$  in the FE phase is significantly lower ( $T \sim 400^\circ\text{C}$ ), and from the device fabrication viewpoint this feature makes application of  $\text{Hf}_{0.5}\text{Zr}_{0.5}\text{O}_2$  films in nonvolatile memory devices extremely promising. In addition, there is a strong correlation between the thickness of the  $\text{Hf}_{0.5}\text{Zr}_{0.5}\text{O}_2$  films and their FE properties.<sup>20</sup> Specifically, among the thin films in the range from 5.5 to 25 nm, the thinner films exhibit higher remnant polarization—effect attributed to the largest volume fraction of the non-centrosymmetric orthorhombic phase.<sup>21</sup> To the best of our knowledge, so far no ferroelectric behavior has been reported for thinner  $\text{HfO}_2$ -based films. Meanwhile, should the ferroelectricity in ultrathin ( $\sim 3\text{--}4$  nm and below) layers persists, it would open an opportunity to design the  $\text{HfO}_2$ -based FTJ devices. Since the polycrystalline hafnium oxide films can be routinely grown directly on the Si substrates, integrated FTJs can be manufactured in the complementary metal–oxide–semiconductor (CMOS) environment. In this work, we report observation of ferroelectricity and testing of the polarization switching behavior in ultrathin ( $\sim 2.5$  nm)  $\text{Hf}_{0.5}\text{Zr}_{0.5}\text{O}_2$  films grown on highly doped Si substrates with TiN top electrodes ultimately targeting the realization of the Si-based FTJ devices. We employ a combination of transmission electron microscopy (TEM) in cross-sectional and plan-view modes along with piezoresponse force microscopy (PFM) and pulse switching techniques to gain insight into the structural and ferroelectric properties of  $\text{Hf}_{0.5}\text{Zr}_{0.5}\text{O}_2$  films. We further use X-ray photoelectron spectroscopy (XPS) data to reveal the peculiarities of electronic structure of  $\text{TiN}/\text{Hf}_{0.5}\text{Zr}_{0.5}\text{O}_2/\text{n}^+\text{-Si}$  prototype stacks necessary for FTJ implementation.

## RESULTS AND DISCUSSION

Ultrathin  $\text{Hf}_{0.5}\text{Zr}_{0.5}\text{O}_2$  films were grown by the atomic layer deposition (ALD) technique on the highly doped n-type Si ( $\rho = 0.005 \Omega\cdot\text{cm}$ ) substrates with a native  $\text{SiO}_2$  layer removed prior to the growth.<sup>22</sup> A TiN overlayer was subsequently deposited by ALD at  $T = 400^\circ\text{C}$ , yielding a crystallized underlying  $\text{Hf}_{0.5}\text{Zr}_{0.5}\text{O}_2$  film (see Supporting Information, section 1). Rutherford backscattering spectrometry data (Figure S1 of the Supporting Information), high-resolution transmission electron microscopy (HRTEM) (Figure S4), and scanning transmission electron microscopy analysis in combination with X-ray energy-dispersive spectrometry (Figures S2 and S3) reveal  $\text{Hf}:\text{Zr}:\text{O} \approx 1:1:4$  stoichiometry and crystalline structure in the 2.5 nm thick Hf–Zr oxide films as well as the presence of a  $\sim 1$  nm thick  $\text{SiO}_x$  layer at the bottom interface.

To gain insight into the structural properties of ultrathin  $\text{Hf}_{0.5}\text{Zr}_{0.5}\text{O}_2$  films on Si, phase identification has been performed using a combination of selected area electron diffraction patterns (SAED), the SAED pattern simulation, high-resolution TEM imaging, and their Fourier transforms (diffractograms) by means of Java Electron Microscopy Software (JEMS).<sup>23</sup> The SAED pattern taken from the plan-view TEM of the  $\text{Hf}_{0.5}\text{Zr}_{0.5}\text{O}_2$  film upon removal of the top TiN layer (Figure 1) shows the polycrystalline nature of the films with the grains possessing orthorhombic and/or monoclinic structures. The best fit between the experimental and calculated SAED patterns was obtained for orthorhombic (o)  $Pbc2_1$ <sup>24</sup> and monoclinic (m)  $P12_1/c1$ <sup>25</sup> phases (the detailed analysis of the SAED pattern is given in Figure S5). Although different phases of the  $\text{Hf}_{0.5}\text{Zr}_{0.5}\text{O}_2$  films (as well as those of binary  $\text{HfO}_2$  and  $\text{ZrO}_2$ ) have very similar unit cell parameters, precluding the accurate phase identification from SAED pattern analysis, the

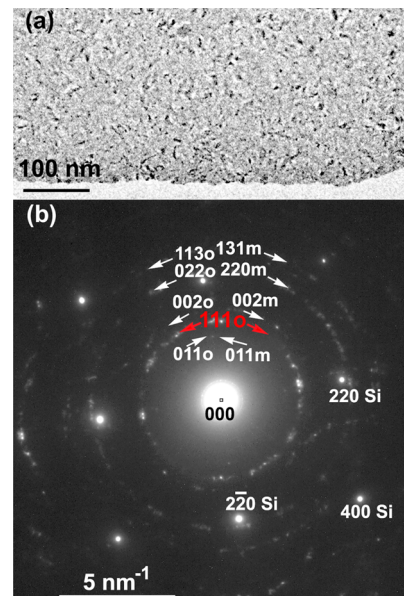


**Figure 1.** (a) Plan-view TEM image of the polycrystalline  $\text{Hf}_{0.5}\text{Zr}_{0.5}\text{O}_2$  film; (b) corresponding SAED pattern with reflections from orthorhombic (reflection label “o”) and monoclinic (reflection label “m”)  $\text{Hf}_{0.5}\text{Zr}_{0.5}\text{O}_2$  and single-crystalline Si substrate (the ring labeled “111o” and marked in red can be attributed to the orthorhombic phase only).

diffraction ring marked with red arrows in Figure 1 can be attributed to only the 111o reflex. We therefore conclude that the orthorhombic phase is present in the  $\text{Hf}_{0.5}\text{Zr}_{0.5}\text{O}_2$  film. For unambiguous identification of the structural phase, the accurate measurements of distances and angles for the corresponding atomic planes in the HRTEM diffractograms from individual grains were performed. The experimental HRTEM images were compared with the simulated ones for different crystalline structures. Such analysis performed on several hundreds of individual  $\text{Hf}_{0.5}\text{Zr}_{0.5}\text{O}_2$  grains reveals that small grains with the linear size of less than 25 nm possess the orthorhombic structure without center of symmetry  $Pbc2_1$ .

One of such grains is shown in Figure 2 along with the corresponding diffractogram taken along the [110] direction and the HRTEM image simulated by the Bloch wave method. It is worth noting that the presence of metastable non-centrosymmetric orthorhombic phase has been recently established in 10 nm-thick ferroelectric  $\text{HfO}_2\text{-Si}$  films by the position-averaged convergent beam electron diffraction method.<sup>18</sup>

The functional FE properties of the 2.5 nm thick  $\text{Hf}_{0.5}\text{Zr}_{0.5}\text{O}_2$  films have been assessed by resonant-enhanced PFM. Figure 3a–c shows the surface morphology of the film along with the PFM amplitude and phase images of the bidomain pattern written by an electrically biased tip. The PFM phase image shows well-defined bright and dark contrast regions with the phase difference of about  $180^\circ$ , which correspond to the upward and downward polarization states, respectively. Strong and stable PFM amplitude signals from the poled regions imply robust remanent polarization. The switching behavior of the  $\text{Hf}_{0.5}\text{Zr}_{0.5}\text{O}_2$  films is illustrated by the local hysteresis PFM loops acquired on the bare film surface (Figure 3d). To quell concerns that this behavior is caused by the effects other than ferroelectric switching (e.g., electrostatic tip–sample interaction or ion migration),<sup>26–28</sup> the PFM hysteresis loops were also

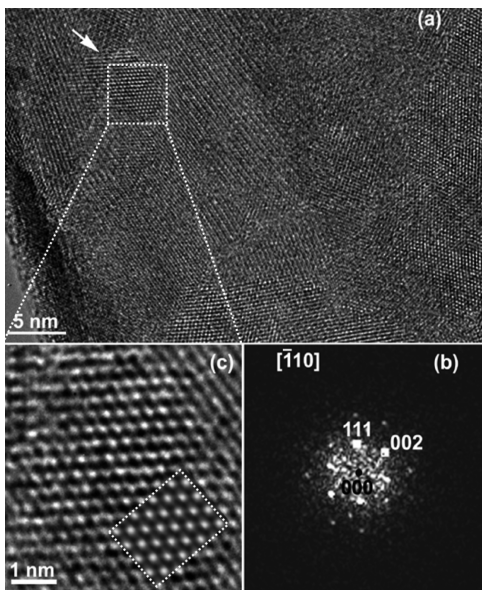


**Figure 2.** (a) HRTEM plan-view image of the polycrystalline  $\text{Hf}_{0.5}\text{Zr}_{0.5}\text{O}_2$  film with the small grain marked by an arrow and a rectangle, (b) HRTEM diffractogram of this grain taken along the  $(1\bar{1}0)$  direction, and (c) the magnified HRTEM image of the small grain with the simulated image in the inset (marked by a dotted rectangle).

measured on the top TiN electrodes (Figure 3e). The FE hysteresis switching behavior is still evident for the TiN/ $\text{Hf}_{0.5}\text{Zr}_{0.5}\text{O}_2/\text{n}^+\text{-Si}$  junction and a strong shift of the loops along the horizontal axis is indicative of its strong asymmetry due to the employment of different electrodes. Although the nominal coercive voltage for this structure derived from the PFM data is about 2 V, it should be noted that the applied voltage is distributed across the TiN/ $\text{Hf}_{0.5}\text{Zr}_{0.5}\text{O}_2/\text{SiO}_x/\text{n}^+\text{-Si}$  stack. The electrostatic modeling of the potential distribution in this metal–oxide–semiconductor (MOS) structure (Supporting Information, Section 4) reveals that the actual coercive voltage

$V_c$  of the 2.5 nm thick  $\text{Hf}_{0.5}\text{Zr}_{0.5}\text{O}_2$  layer is about 0.8 V (Figures S8 and S9).

Finally, the spontaneous polarization value has been evaluated by measuring the switching currents using a standard pulse switching technique called PUND (Positive Up Negative Down), which allows separating a current signal associated with polarization reversal from the parasitic signal due to dielectric charging.<sup>29–31</sup> Figure 3f shows the typical PUND measurement results for a 7  $\mu\text{m}$  diameter TiN/ $\text{Hf}_{0.5}\text{Zr}_{0.5}\text{O}_2/\text{SiO}_x/\text{n}^+\text{-Si}$  capacitor switched by 5 V, 2  $\mu\text{s}$  voltage pulse. The transient current  $I_s$  in response to the application of the first voltage pulse consists of the polarization switching current  $I_{ps}$  and the loading (nonswitching) current  $I_{ns}$ , which is measured during application of the second voltage pulse (Figure S11 and supporting data in the Supporting Information, section 5). Integration of the  $I_{ps}$  signal, which was found as a difference between  $I_s$  and  $I_{ns}$ , yielded the switchable polarization value of around 2.5–3.5  $\mu\text{C}/\text{cm}^2$ . Although this value is significantly smaller than the record polarization of 17  $\mu\text{C}/\text{cm}^2$  reported for  $\text{Hf}_{0.5}\text{Zr}_{0.5}\text{O}_2$  thin films,<sup>19</sup> its importance is in the unambiguous demonstration of the ferroelectric nature of the 2.5 nm thick  $\text{Hf}_{0.5}\text{Zr}_{0.5}\text{O}_2$  films. The polarization reversal time measured here is less than 30 ns and further studies are underway to investigate the voltage-dependent switching dynamics of the films.

To elucidate the information on the chemical properties of the  $\text{Hf}_{0.5}\text{Zr}_{0.5}\text{O}_2$  bottom interface with the Si substrate and to characterize the band lineup at the upper TiN/ $\text{Hf}_{0.5}\text{Zr}_{0.5}\text{O}_2$  interface, we performed in situ XPS analysis. Si 2p core-level spectrum from the surface of the  $\text{n}^+\text{-Si}$  substrate upon removal of native oxide prior to the ALD growth is shown in Figure 4a. It can be perfectly fitted with a single doublet with the binding energy (BE) of Si  $2p_{3/2}$  line  $\sim 99.7$  eV, spin–orbit split of 0.6 eV, and line width of fwhm  $\approx 0.7$  eV attributed to the monocrystalline  $\text{n}^+\text{-Si}$ , with no traces of  $\text{SiO}_2$ . The growth of  $\text{Hf}_{0.5}\text{Zr}_{0.5}\text{O}_2$  layer on Si gives rise to the formation of sub-nanometer thick interfacial  $\text{SiO}_2$  layer, which is evident from the higher energy spectral component shifted by about 3.2 eV

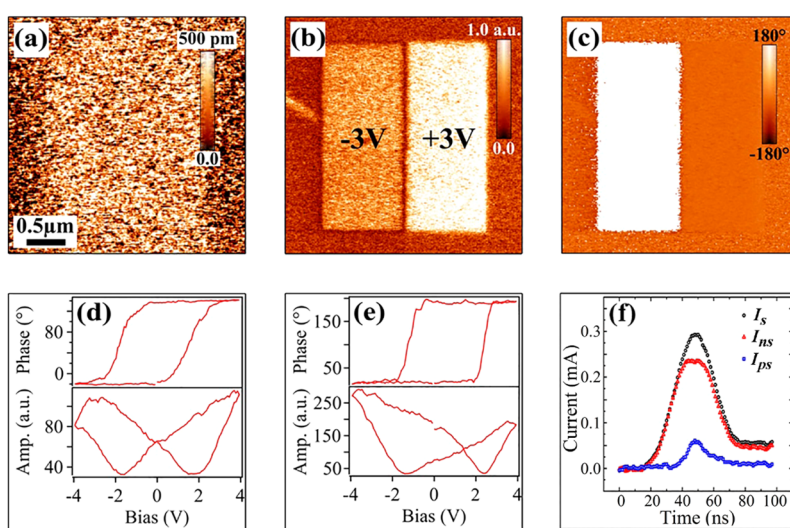


**Figure 3.** (a) Local morphology (a) and (b, c) PFM amplitude (b) and phase (c) images of the 2.5 nm thick  $\text{Hf}_{0.5}\text{Zr}_{0.5}\text{O}_2$  film on the  $\text{n}^+\text{-Si}$  substrate. Bright/dark rectangular regions in (c) correspond to the areas poled upward/downward by the tip bias of  $-3$  V/3 V. (d, e) PFM phase and amplitude hysteresis loops taken on the bare  $\text{Hf}_{0.5}\text{Zr}_{0.5}\text{O}_2$  surface (d) and on the TiN top electrode (e). (f) “Positive Up Negative Down” data showing three types of current signals measured in the TiN/ $\text{Hf}_{0.5}\text{Zr}_{0.5}\text{O}_2/\text{SiO}_x/\text{n}^+\text{-Si}$  capacitor: transient current  $I_s$ , loading (nonswitching) current  $I_{ns}$ , and polarization switching current  $I_{ps}$ . See details in the text.

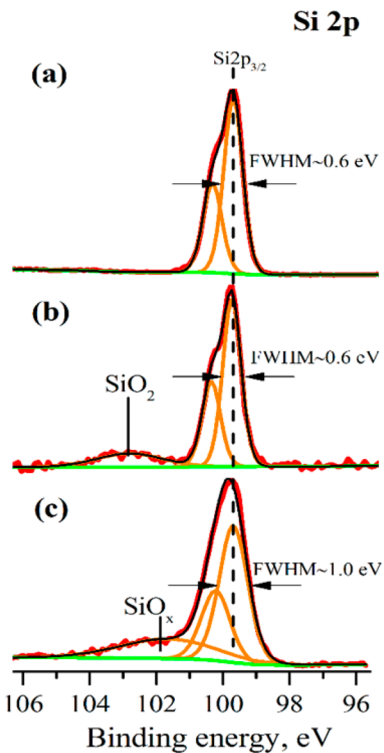


**Figure 4.** Si 2p core level spectra measured (a) from HF last  $n^+$ -Si surface prior to the growth, (b) upon ALD growth of a 2.5 nm thick  $\text{Hf}_{0.5}\text{Zr}_{0.5}\text{O}_2$  film, and (c) upon ALD growth of the capping TiN layer and its further  $\text{Ar}^+$  ion etching.

from the main  $\text{Si} 2\text{p}_{3/2}$  line (Figure 4b).  $\text{Si} 2\text{p}$  spectrum taken upon the growth of the capping TiN layer on top of  $\text{Hf}_{0.5}\text{Zr}_{0.5}\text{O}_2$  and its subsequent partial removal by ion etching reveals a slightly increased intensity and the shift of the peak attributed to  $\text{SiO}_x$  toward the lower binding energy. With use of well-known methodology<sup>32</sup> and inelastic mean free paths of  $\text{Si} 2\text{p}$  photoelectrons in  $\text{Si}$  and  $\text{SiO}_2$  of 1.6 and 2.6 nm, respectively,<sup>33</sup> the thickness of  $\text{SiO}_x$  interfacial layer formed upon TiN growth on top of  $\text{Hf}_{0.5}\text{Zr}_{0.5}\text{O}_2$  is found to be  $\sim 1$  nm, which is consistent with cross-sectional TEM data. In addition, the significant broadening of  $\text{Si}^0$  line is observed (cf. fwhm  $\sim 1$  eV vs 0.6 eV prior to the TiN growth), which points to the nonuniform potential distribution across the adjacent  $\text{Si}$

substrate probed by XPS. The thickness of the space charge region for the highly doped ( $n \approx 10^{19} \text{ cm}^{-3}$ )  $\text{Si}$  substrate is estimated to be about 15 nm. We believe that the charge accumulation in  $\text{Si}$  and the corresponding potential distribution is caused by the electrical field originating from the polarization charges of  $\text{Hf}_{0.5}\text{Zr}_{0.5}\text{O}_2$  at the bottom interface. The modeling of the line broadening caused by the potential distribution (band bending) across the space charge region of  $\text{Si}$  probed by XPS (Figure S10) confirms the validity of such hypothesis and is taken as additional evidence of the formation of a ferroelectric phase in  $\text{Hf}_{0.5}\text{Zr}_{0.5}\text{O}_2$ .

For future implementation of  $\text{Si}$ -based FTJs, it is critically important to design the optimized potential barrier profile. To gain quantitative information on the electronic properties of  $\text{TiN}/\text{Hf}_{0.5}\text{Zr}_{0.5}\text{O}_2/n^+$ - $\text{Si}$  stack, we further characterized the band lineup at the upper  $\text{TiN}/\text{Hf}_{0.5}\text{Zr}_{0.5}\text{O}_2$  interface. (The related properties of the bottom  $\text{Hf}_{0.5}\text{Zr}_{0.5}\text{O}_2/\text{Si}$  interface are the subject of further studies and will be reported separately.) To determine the electronic band alignment at the top  $\text{TiN}/\text{Hf}_{0.5}\text{Zr}_{0.5}\text{O}_2$  interface, we employed the well-known XPS-based methodology reported previously.<sup>34,35</sup> The valence band offset (VBO) can be calculated as follows (Figure 5a):

$$\text{VBO} = (\text{BE}_{\text{Ti}2\text{p}} - E_F)_{\text{TiN}} - (\text{BE}_{\text{Ti}2\text{p}} - \text{BE}_{\text{Hf}4\text{f}})_{\text{HfO}_2/\text{TiN}} - (\text{BE}_{\text{Hf}4\text{f}} - \text{VBM})_{\text{HfO}_2} \quad (1)$$

$\text{BE}_{\text{Hf}4\text{f}}$  line separation with respect to the valence band maximum (VBM) for the bulk  $\text{Hf}_{0.5}\text{Zr}_{0.5}\text{O}_2$  is  $(E_{\text{Hf}4\text{f}} - \text{VBM}) = 14.1$  eV (Supporting Information, Figure S6). The line separation  $(\text{BE}_{\text{Ti}2\text{p}} - \text{BE}_{\text{Hf}4\text{f}})_{\text{HfO}_2/\text{TiN}}$  of 438.0 eV is measured upon the growth of a 3 nm thick capping TiN layer on top of the  $\text{Hf}_{0.5}\text{Zr}_{0.5}\text{O}_2/n^+$ - $\text{Si}$  sample, while the energy difference  $\text{BE}_{\text{Ti}2\text{p}} - E_F$  is just a position of the  $\text{Ti} 2\text{p}$  peak at  $\text{BE}_{\text{Ti}2\text{p}} = 455.4$  eV (Figure 5b).

$\text{Ti} 2\text{p}$  spectrum can be fitted with three spin-orbit split lines. The first one with  $\text{Ti} 2\text{p}_{3/2}$  component at  $\text{BE} = 455.4$  eV (1) is attributed to the metallic TiN.<sup>36</sup> Positions of the additional  $\text{Ti} 2\text{p}_{3/2}$  components at  $\text{BE} = 456.4$  eV (2) and 457.8 eV (3) point out the formation of  $\text{TiON}$  and nonstoichiometric  $\text{TiO}_{2-x}$  subsurface layers, respectively.<sup>37</sup> The  $\text{Hf} 4\text{f}$  spectrum is dominated by the spin-orbit split doublet with the  $\text{Hf} 4f_{7/2}$  line binding energy  $\text{BE} = 17.4$  eV corresponding to the stoichiometric  $\text{HfO}_2$ . The spectral component with the lower

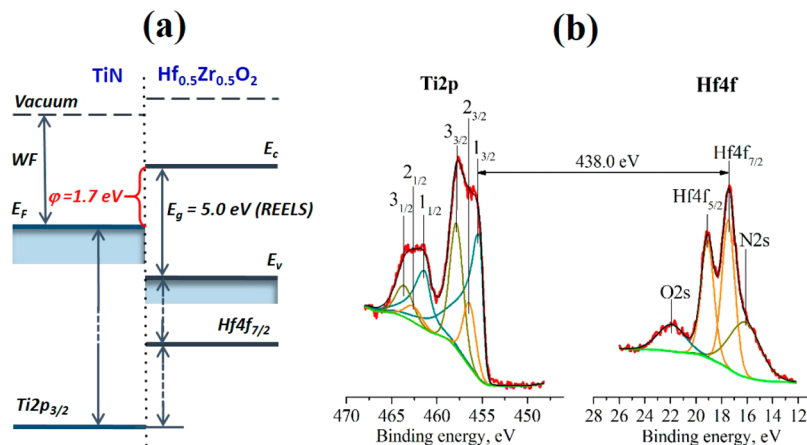


**Figure 5.** (a) Schematic diagram of the band offset at the  $\text{TiN}/\text{Hf}_{0.5}\text{Zr}_{0.5}\text{O}_2$  interface; (b) separation between  $\text{Ti} 2\text{p}$  and  $\text{Hf} 4\text{f}$  core-level lines as measured on the 3 nm thick TiN layer ALD grown on top of the  $\text{Hf}_{0.5}\text{Zr}_{0.5}\text{O}_2/\text{Si}$  sample.

binding energy ( $\text{BE} = 16.1$  eV) belongs to N 2s core-level line, while the spectral component with the higher binding energy is attributed to the O 2s line ( $\text{BE} = 21.9$  eV). According to the employed method,<sup>35</sup> the position of the Hf 4f line is defined by the effective work function  $\text{WF}_{\text{eff}}$  of a grounded metal (TiN) electrode in contact with a dielectric ( $\text{Hf}_{0.5}\text{Zr}_{0.5}\text{O}_2$ ), and  $\text{BE}_{\text{Hf 4f}} = 17.4$  eV corresponds to the effective work function of 4.8 eV for TiN. This value is larger compared to the TiN work function of 4.4–4.6 eV reported previously,<sup>38</sup> which means that an electric dipole has built up at the TiN/ $\text{Hf}_{0.5}\text{Zr}_{0.5}\text{O}_2$  interface, with the positive charges at the TiN electrode. This result corroborates the conclusion, which can be made from PFM data, that the polarization in as-grown  $\text{Hf}_{0.5}\text{Zr}_{0.5}\text{O}_2$  film has a tendency to point toward the Si substrate (Figure 3e).

Calculation of the valence band offset (VBO) in  $\text{Hf}_{0.5}\text{Zr}_{0.5}\text{O}_2$  in contact with TiN according to eq 1 yielded a value of 3.3 eV. Taking into account the energy band gap  $E_g \approx 5.0$  eV of the 2.5 nm thick  $\text{Hf}_{0.5}\text{Zr}_{0.5}\text{O}_2$  layer measured separately by reflected electron energy loss spectroscopy (REELS) (Figure S7), the conduction band offset, which is the potential energy barrier height  $\varphi$  at the top interface, is 1.7 eV (Figure 5a).

To enable a tunneling electroresistance (TER) effect, one has to modulate the potential barrier height across a tunneling-transparent ferroelectric layer by means of polarization reversal. In addition, a greatly enhanced TER effect can be expected if, in parallel with the height, the barrier width is modulated. Indeed, in the case of the FTJs with a semiconducting electrode, its space charge region can be switched between accumulation and depletion of majority carriers by switching of polarization, giving rise to a large variation of the effective barrier width and the giant TER effect.<sup>39</sup> In the case of a highly doped Si used as an electrode in  $\text{Hf}_{0.5}\text{Zr}_{0.5}\text{O}_2$ -based FTJs, careful band engineering across the metal-ferroelectric-Si stack is required, which involves simultaneous optimization of the effective work function of the top electrode in contact with the  $\text{Hf}_{0.5}\text{Zr}_{0.5}\text{O}_2$  layer, control of the carrier type, and the doping level of the Si substrate as well as possible electrode dipole built up in the interfacial  $\text{SiO}_x$  layer. This work is currently underway.

## CONCLUSION

We have succeeded in fabrication of ultrathin  $\text{Hf}_{0.5}\text{Zr}_{0.5}\text{O}_2$  ferroelectric films with the thickness of just 2.5 nm, which makes them compatible with FTJ devices based on the tunneling electroresistance effect. Structural and functional characterization of the films by TEM and PFM techniques, respectively, confirms the formation of the stable and switchable ferroelectric phase. Analysis of the electronic band lineup at the top TiN/ $\text{Hf}_{0.5}\text{Zr}_{0.5}\text{O}_2$  interface and band bending at the bottom  $n^+$ -Si layer attributed to the presence of the polarization charges further corroborate the ferroelectric nature of the ultrathin  $\text{Hf}_{0.5}\text{Zr}_{0.5}\text{O}_2$  films. The obtained results show that hafnium oxide films can be successfully grown directly on the Si substrates, which paves the way for CMOS fabrication of the integrated  $\text{Hf}_{0.5}\text{Zr}_{0.5}\text{O}_2$ -based FTJ devices. Further efforts are aimed at the investigation of the mechanism of polarization reversal and resistive switching behavior in the  $\text{Hf}_{0.5}\text{Zr}_{0.5}\text{O}_2$  films and optimization of their interface properties, which play a critical role in the resistive switching effect.

## ASSOCIATED CONTENT

### Supporting Information

The Supporting Information is available free of charge on the ACS Publications website at DOI: [10.1021/acsami.5b11653](https://doi.org/10.1021/acsami.5b11653).

Additional information and figures related to the growth and characterization of the ferroelectric  $\text{Hf}_{0.5}\text{Zr}_{0.5}\text{O}_2$  films (PDF)

## AUTHOR INFORMATION

### Corresponding Authors

\*E-mail: [agrerverman2@unl.edu](mailto:agrerverman2@unl.edu) (A.G.).

\*E-mail: [zenkevich.av@mpt.ru](mailto:zenkevich.av@mpt.ru) (A.Z.).

### Notes

The authors declare no competing financial interest.

## ACKNOWLEDGMENTS

This work was supported from the Russian Science Foundation Grant No. 14-19-01698. Research at the University of Nebraska was supported by the National Science Foundation (NSF) through the Nebraska Materials Research Science and Engineering Center (MRSEC) under Grant No. DMR-1420645. A.G. also acknowledges the support of the Nanoelectronics Research Corporation (NERC), a wholly-owned subsidiary of the Semiconductor Research Corporation (SRC), through the Center for Nanoferroic Devices (CNFD), an SRC-NRI Nanoelectronics Research Initiative Center under Task ID 2398.002. E.S. is deeply indebted to Prof. Cécile Hebert for kindly providing access to the microscopes and the software of the Centre Interdisciplinaire de Microscopie Electronique of EPFL, Prof. P. A. Buffat for the discussion of the results, and Mrs. D. Laub for help in the sample preparation.

## REFERENCES

- Bune, A. V.; Fridkin, V. M.; Ducharme, S.; Blinov, L. M.; Palto, S. P.; Sorokin, A. V.; Yudin, S. G.; Zlatkin, A. Two-Dimensional Ferroelectric Films. *Nature* **1998**, *391*, 874–877.
- Streiffer, S. K.; Eastman, J. A.; Fong, D. D.; Thompson, C.; Munkholm, A.; Ramana Murty, M. V.; Auciello, O.; Bai, G. R.; Stephenson, G. B. Observation of Nanoscale 180° Stripe Domains in Ferroelectric PbTiO<sub>3</sub> Thin Films. *Phys. Rev. Lett.* **2002**, *89*, 067601.
- Fong, D. D.; Stephenson, G. B.; Streiffer, S. K.; Eastman, J. A.; Auciello, O.; Fuoss, P. H.; Thompson, C. Ferroelectricity in Ultrathin Perovskite Films. *Science* **2004**, *304*, 1650–1653.
- Garcia, V.; Fusil, S.; Bouzehouane, K.; Enouz-Vedrenne, S.; Mathur, N. D.; Barthélémy, A.; Bibes, M. Giant Tunnel Electroresistance for Non-Destructive Readout of Ferroelectric States. *Nature* **2009**, *460*, 81–84.
- Junquera, J.; Ghosez, P. Critical Thickness for Ferroelectricity in Perovskite Ultrathin Films. *Nature* **2003**, *422*, 506–509.
- Tsybaly, E. Y.; Kohlstedt, H. Tunneling Across a Ferroelectric. *Science* **2006**, *313*, 181–183.
- Kohlstedt, H.; Pertsev, N. A.; Rodríguez Contreras, J.; Waser, R. Theoretical Current-Voltage Characteristics of Ferroelectric Tunnel Junctions. *Phys. Rev. B: Condens. Matter Mater. Phys.* **2005**, *72*, 125341.
- (8) Gruverman, A.; Wu, D.; Lu, H.; Wang, Y.; Jang, H. W.; Folkman, C. M.; Zhuravlev, M.; Felker, D.; Rzchowski, M.; Eom, C.-B.; Tsybaly, E. Y. Tunneling Electroresistance Effect in Ferroelectric Tunnel Junctions at the Nanoscale. *Nano Lett.* **2009**, *9*, 3539–3543.
- Chanthbouala, A.; Crassous, A.; Garcia, V.; Bouzehouane, K.; Fusil, S.; Moya, X.; Allibe, J.; Dlubak, B.; Grollier, J.; Xavier, S.; Deranlot, C.; Moshar, A.; Proksch, R.; Mathur, N. D.; Bibes, M.; Barthélémy, A. Solid-State Memories Based on Ferroelectric Tunnel Junctions. *Nat. Nanotechnol.* **2012**, *7*, 101–104.
- Gao, S.; Liu, J. M.; Au, K.; Dai, J. Y. Nanoscale Ferroelectric Tunnel Junctions Based on Ultrathin BaTiO<sub>3</sub> Film and Ag Nanoelectrodes. *Appl. Phys. Lett.* **2012**, *101*, 142905.
- Zenkevich, A.; Minnekaev, M.; Matveyev, Y.; Lebedinskii, Y.; Bulakh, K.; Chouprik, A.; Baturin, A.; Maksimova, K.; Thiess, S.; Drube, W. Electronic Band Alignment and Electron Transport in Cr/

- BaTiO<sub>3</sub>/Pt Ferroelectric Tunnel Junctions. *Appl. Phys. Lett.* **2013**, *102*, 062907.
- (12) Garcia, V.; Bibes, M. Ferroelectric Tunnel Junctions for Information Storage and Processing. *Nat. Commun.* **2014**, *5*, 4289.
- (13) Mueller, S.; Mueller, J.; Singh, A.; Riedel, S.; Sundqvist, J.; Schroeder, U.; Mikolajick, T. Incipient Ferroelectricity in Al-Doped HfO<sub>2</sub> Thin Films. *Adv. Funct. Mater.* **2012**, *22*, 2412–2417.
- (14) Schröder, U.; Yurchuk, E.; Müller, J.; Martin, D.; Schenk, T.; Polakowski, P.; Adelmann, C.; Popovici, M. I.; Kalinin, S. V.; Mikolajick, T. Impact of Different Dopants on the Switching Properties of Ferroelectric Hafnium Oxide. *Jpn. J. Appl. Phys.* **2014**, *53*, 08LE02.
- (15) Müller, J.; Polakowski, P.; Mueller, S.; Mikolajick, T. Ferroelectric Hafnium Oxide Based Materials and Devices: Assessment of Current Status and Future Prospects. *ECS Trans.* **2014**, *64*, 159–168.
- (16) Clima, S.; Wouters, D. J.; Adelmann, C.; Schenk, T.; Schröder, U. U.; Jurczak, M.; Pourtois, G. Identification of the Ferroelectric Switching Process and Dopant-Dependent Switching Properties in Orthorhombic HfO<sub>2</sub>: A first principles insight. *Appl. Phys. Lett.* **2014**, *104*, 092906.
- (17) Zhou, D.; Müller, J.; Xu, J.; Knebel, S.; Bräuhaus, D.; Schröder, U. Insights into Electrical Characteristics of Silicon Doped Hafnium Oxide Ferroelectric Thin Films. *Appl. Phys. Lett.* **2012**, *100*, 082905.
- (18) Sang, X.; Grimley, E. D.; Schenk, T.; Schroeder, U.; LeBeau, J. M. On the Structural Origins of Ferroelectricity in HfO<sub>2</sub> Thin Films. *Appl. Phys. Lett.* **2015**, *106*, 162905.
- (19) Müller, J.; Böscke, T. S.; Schröder, U.; Mueller, S.; Bräuhaus, D.; Böttger, U.; Frey, L.; Mikolajick, T. Ferroelectricity in Simple Binary ZrO<sub>2</sub> and HfO<sub>2</sub>. *Nano Lett.* **2012**, *12*, 4318.
- (20) Müller, J.; Böscke, T. S.; Bräuhaus, D.; Schröder, U.; Böttger, U.; Sundqvist, J.; Kucher, P.; Mikolajick, T.; Frey, L. Phase Transitions in Ferroelectric Silicon Doped Hafnium Oxide. *Appl. Phys. Lett.* **2011**, *99*, 112901.
- (21) Park, M. H.; Kim, H. J.; Kim, Y. J.; Lee, W.; Moon, T.; Hwang, C. S. Evolution of Phases and Ferroelectric Properties of Thin Hf<sub>0.5</sub>Zr<sub>0.5</sub>O<sub>2</sub> Films According to the Thickness and Annealing Temperature. *Appl. Phys. Lett.* **2013**, *102*, 242905.
- (22) Chernikova, A.; Kozodaev, M.; Markeev, A.; Matveev, Yu.; Negrov, D.; Orlov, O. Confinement-free Annealing Induced Ferroelectricity in Hf<sub>0.5</sub>Zr<sub>0.5</sub>O<sub>2</sub> Thin Films. *Microelectron. Eng.* **2015**, *147*, 15–18.
- (23) Java Electron Microscopy Software (JEMS). <http://www.jems-saas.ch/> (accessed March 10, 2016).
- (24) Kisi, E. H.; Howard, C. J.; Hill, R. J. Crystal Structure of Orthorhombic Zirconia in Partially Stabilized Zirconia. *J. Am. Ceram. Soc.* **1989**, *72*, 1757–1760.
- (25) Smith, D. K.; Newkirk, H. W. The crystal structure of Baddeleite Monoclinic ZrO<sub>2</sub> and Its Relation to the Polymorphism of ZrO<sub>2</sub>. *Acta Crystallogr.* **1965**, *18*, 983–991.
- (26) Borowiak, A. S.; Baboux, N.; Albertini, D.; Vilquin, B.; Girons, G. S.; Pelloquin, S.; Gautier, B. Electromechanical Response of Amorphous LaAlO<sub>3</sub> Thin Film Probed by Scanning Probe Microscopies. *Appl. Phys. Lett.* **2014**, *105*, 012906.
- (27) Kalinin, S. V.; Bonnell, D. A. Contrast Mechanism Maps for Piezoresponse Force Microscopy. *J. Mater. Res.* **2002**, *17*, 936–939.
- (28) Sharma, P.; Ryu, S.; Burton, J. D.; Paudel, T. R.; Bark, C. W.; Huang, Z.; Ariando; Tsymbal, E. Y.; Catalan, G.; Eom, C. B.; Gruverman, A. Mechanical Tuning of LaAlO<sub>3</sub>/SrTiO<sub>3</sub> Interface Conductivity. *Nano Lett.* **2015**, *15*, 3547–3551.
- (29) Scott, J. F.; Kammerdiner, L.; Parris, M.; Traynor, S.; Ottenbacher, V.; Shawabkeh, A.; Oliver, W. F. Switching Kinetics of Lead Zirconate Titanate Submicron Thin-Film Memories. *J. Appl. Phys.* **1988**, *64*, 787–792.
- (30) Dehoff, C.; Rodriguez, B. J.; Kingon, A. I.; Nemanich, R. J.; Gruverman, A.; Cross, J. S. Atomic Force Microscopy-Based Experimental Setup for Studying Domain Switching Dynamics in Ferroelectric Capacitors. *Rev. Sci. Instrum.* **2005**, *76*, 023708.
- (31) Stamm, A.; Kim, D. J.; Lu, H.; Bark, C. W.; Eom, C. B.; Gruverman, A. Polarization Relaxation Kinetics in Ultrathin Ferroelectric Capacitors. *Appl. Phys. Lett.* **2013**, *102*, 092901.
- (32) Lu, Z. H.; McCaffrey, J. P.; Brar, B.; Wilk, G. D.; Wallace, R. M.; Feldman, L. C.; Tay, S. P. SiO<sub>2</sub> Film Thickness Metrology by X-Ray Photoelectron Spectroscopy. *Appl. Phys. Lett.* **1997**, *71*, 2764–2766.
- (33) Hochella, M. F.; Carim, A. H. A Reassessment of Electron Escape Depths in Silicon and Thermally Grown Silicon Dioxide Thin Films. *Surf. Sci.* **1988**, *197*, L260–L268.
- (34) Kraut, E.; Grant, R.; Waldrop, J.; Kowalczyk, S. Precise Determination of the Valence-Band Edge in X-Ray Photoemission Spectra: Application to Measurement of Semiconductor Interface Potentials. *Phys. Rev. Lett.* **1980**, *44*, 1620–1623.
- (35) Lebedinskii, Y.; Zenkevich, A.; Gusev, E. P. Measurements of Metal Gate Effective Work Function by X-Ray Photoelectron Spectroscopy. *J. Appl. Phys.* **2007**, *101*, 074504.
- (36) Doniach, S.; Sunjic, M. Many-Electron Singularity in X-Ray Photoemission and X-Ray Line Spectra from Metals. *J. Phys. C: Solid State Phys.* **1970**, *C3*, 285–291.
- (37) Saha, N. C.; Tompkins, H. G. Titanium Nitride Oxidation Chemistry: An X-Ray Photoelectron Spectroscopy Study. *J. Appl. Phys.* **1992**, *72*, 3072–3079.
- (38) Yagishita, A.; Saito, T.; Nakajima, K.; Inumiya, S.; Matsuo, K.; Shibata, T.; Tsunashima, Y.; Suguro, K.; Arikado, T. Improvement of Threshold Voltage Deviation in Damascene Metal Gate Transistors. *IEEE Trans. Electron Devices* **2001**, *48*, 1604–1611.
- (39) Wen, Z.; Li, C.; Wu, D.; Li, A.; Ming, N. Ferroelectric-Field-Effect-Enhanced Electroresistance in Metal/Ferroelectric/Semiconductor Tunnel Junctions. *Nat. Mater.* **2013**, *12*, 617–621.